Advances in Continuous and Discrete Models

RESEARCH Open Access

Pattern formation in a fractional-order reaction-diffusion predator-prey model with Holling-III functional response

Zhaohua Wu[1], Zhiming Wang[2], Yongli Cai[3], Hongwei Yin[4] and Weiming Wang[1*]

*Correspondence:
wangwm_math@hytc.edu.cn
[1]School of Mathematics and Statistics, Huaiyin Normal University, Huaian, 223300, P.R. China
Full list of author information is available at the end of the article

Abstract

In this paper, we investigate the spatiotemporal dynamics of a fractional-order predator-prey reaction-diffusion model (frPDE) with Holling-type III functional response. We prove that this is not the integer-order reaction-diffusion model, but the frPDE model exhibits fraction-diffusion-induced instability (i.e., Turing instability), which is induced by the fractional-order and diffusion together. Furthermore, via numerical simulations, the frPDE model dynamics exhibits both fractional-order and diffusion controlled Turing pattern formation, which shows that the dynamics of the frPDE model is not simple, but rich and complex.

Keywords: Fractional-order; Holling type III functional response; Fraction-diffusion-induced instability; Pattern formation

1 Introduction

Pattern formation, Turing's pioneering work in 1952 [1], has become a very active area of research, motivated in part by the realization that there are many common aspects of patterns formed by diverse physical, chemical, and biological systems and by reaction-diffusion equations [2]. Understanding the pattern formation of interacting species is significant interest in conservation of biology, ecology and biochemical reactions [3, 4].

It is well known that the predator-prey model plays a major role in the studies of biological invasion of foreign species or epidemic spreading [5]. Among these, the classic predator-prey model with Holling-type III functional response can be described by the following ordinary differential equations (ODEs) [6–8]:

$$\begin{cases} \dfrac{\mathrm{d}u}{\mathrm{d}t} = ru\left(1-\dfrac{u}{k}\right) - \dfrac{qu^2v}{u^2+a}, \\ \dfrac{\mathrm{d}v}{\mathrm{d}t} = -cv + \dfrac{pu^2v}{u^2+a}, \end{cases} \tag{1}$$

where $u(t)$ and $v(t)$ respectively describe the prey's and predator's densities at time t, a is the prey's density at which the predator has the maximum kill rate, q the consumption

rate, $\frac{p}{q}$ the conversion efficiency, c death rate of the predator, k the carrying capacity of the environment, r the intrinsic growth rate. All parameters of the reaction term are positive constants.

The corresponding reaction-diffusion model to model (1) is

$$\begin{cases} \dfrac{\partial u}{\partial t} = d_1 \Delta u + ru\left(1 - \dfrac{u}{k}\right) - \dfrac{qu^2 v}{u^2 + a}, \\ \dfrac{\partial v}{\partial t} = d_2 \Delta v - cv + \dfrac{pu^2 v}{u^2 + a}, \end{cases} \tag{2}$$

where the Laplacian operator Δ describes the random diffusion of these two species from the higher density region to the lower, and the diffusion coefficients d_1 and d_2 are positive.

For simplicity, we call model (1) as ODE model, and (2) as PDE model. Obviously, these two models have the same equilibria. And we sign the positive equilibrium as $E^* = (u^*, v^*)$.

Turing instability According to Turing's idea [1], if the positive equilibrium $E^* = (u^*, v^*)$ is stable for ODE model (1), but unstable with respect to solutions in the case $d_1 > 0$ and $d_2 > 0$ for PDE model (2), then E^* is called diffusion-driven instability (i.e., Turing instability), and model (2) may exhibit stationary Turing pattern.

Unfortunately, for PDE model (2), $E^* = (u^*, v^*)$ is stable when $d_1 > 0$ and $d_2 > 0$, and hence there is nonexistence of diffusion-driven instability, and the model cannot exhibit any stationary pattern [9, 10].

On the other hand, in recent years, much attention has been paid to incorporate fractional derivatives in the population models. Typically, the fractional derivatives are incorporated in an *ad hoc* way by replacing integer order time derivatives with Caputo fractional derivatives directly [11–14]. These models and their analysis are mathematically interesting, and there are some motivations for incorporating memory effects [13]. And a number of fractional-order reaction-diffusion models have been formulated to describe the impact of diffusion on Turing instability and pattern formation [15–21]. Biomathematics experts currently focus on two types of fractional-order reaction-diffusion predator-prey systems: one is to use fractional-order operators to represent the rate of change of population density [15–17], and the other is to use the fractional-order diffusion operator to represent the integer-order in the reaction-diffusion models [18–21]. However, the integer-order models corresponding to these fractional-order models already exhibit Turing instability, and the introduction of fractional order has no substantial impact on the pattern formation. It is worth pointing out that, in [10], Yin et al. investigated the Turing instability of a fractional-order reaction-diffusion predator-prey model.

Based on the discussions above, in the present paper, we investigate the Turing instability of the fractional-order reaction-diffusion predator-prey model with Holling III functional response:

$$\begin{cases} \dfrac{\partial^\eta u}{\partial t^\eta} = d_1 \Delta u + ru\left(1 - \dfrac{u}{k}\right) - \dfrac{qu^2 v}{u^2 + a}, \\ \dfrac{\partial^\eta v}{\partial t^\eta} = d_2 \Delta v - cv + \dfrac{pu^2 v}{u^2 + a}, \end{cases} \tag{3}$$

with the positive initial conditions:

$$u(x, 0) > 0, v(x, 0) > 0, x \in \Omega,$$

and the zero-flux boundary conditions:

$$\frac{\partial u}{\partial \boldsymbol{\upsilon}} = \frac{\partial v}{\partial \boldsymbol{\upsilon}} = 0, x \in \partial\Omega,$$

where $\eta \in (0,1)$, $u(x,t)$ and $v(x,t)$ respectively describe the prey's and predator's densities at time t on the spatial position x. Ω is the bounded open domain in $\mathbb{R}^n$, $\boldsymbol{\upsilon}$ the outward unit normal vector on $\partial\Omega$. We will study the stability and obtain the conditions of the Turing instability for system (3).

And the corresponding ODE model is

$$\begin{cases} \dfrac{\mathrm{d}^\eta u}{\mathrm{d}t^\eta} = ru\left(1-\dfrac{u}{k}\right) - \dfrac{qu^2 v}{u^2+a}, \\ \dfrac{\mathrm{d}^\eta v}{\mathrm{d}t^\eta} = -cv + \dfrac{pu^2 v}{u^2+a}, \end{cases} \tag{4}$$

where $\dfrac{\mathrm{d}^\eta u}{\mathrm{d}t^\eta}$ is the standard Caputo's partial derivative with respect to the time variable t as follows:

$$\frac{\mathrm{d}^\eta u}{\mathrm{d}t^\eta} = \frac{1}{\Gamma(1-\eta)} \int_0^t \frac{\mathrm{d}u(s)}{\mathrm{d}s} \frac{\mathrm{d}s}{(t-s)^\eta}.$$

For simplicity, we call model (3) as frPDE model, and (4) as frODE model.

The main goal of this paper is to make an insight into the instability induced by the fractional-order in model (3). Our main interest is to check whether the fractional-order is a plausible mechanism of developing spatiotemporal pattern in model (3).

The rest of this article is organized as follows: In Sect. 2, we give the stability/instability analysis of the models. In Sect. 3, we illustrate typical Turing patterns via numerical simulations. Finally, conclusions and remarks are presented in Sect. 4.

2 Stability analysis

Easy to know that ODE model (1), PDE model (2) and frODE model (4), frPDE model (3) have the same equilibria as follows:

1) Extinction equilibrium: $E_0 = (0,0)$ (the predator and the prey go extinct);

2) Boundary equilibrium: $E_1 = (k,0)$ (the prey dies out);

3) Coexistence equilibrium: if $p > c\left(1+\dfrac{a}{k^2}\right)$, the model exhibits a unique positive equilibrium $E^* = (u^*, v^*)$ (the predator and the prey exist), where

$$u^* = \sqrt{\frac{ac}{p-c}}, \quad v^* = \frac{apr(k\sqrt{p-c} - \sqrt{ac})}{kq\sqrt{ac}(p-c)}.$$

It should be pointed out that the focus of the present paper is on Turing instability and hence we only study the stability of the coexistence equilibrium E^* in the remainder.

2.1 The case of integer-order models

Theorem 2.1 *For ODE model (1), assume that $p > c\left(1+\dfrac{a}{k^2}\right)$, i.e., there is a unique positive equilibrium $E^* = (u^*, v^*)$. Then E^* is stable if either of the following inequalities holds*:

(H_1) $a \geq k^2$;

(H_2) $a < k^2$ *and* $kp + 2c\sqrt{\dfrac{ac}{p-c}} > 2kc$.

Proof The Jacobian matrix of ODE (1) at E^* is

$$J = \begin{pmatrix} J_{11} & J_{12} \\ J_{21} & 0 \end{pmatrix} = \begin{pmatrix} \frac{2r\left(k\left(c-\frac{p}{2}\right)-c\sqrt{\frac{ac}{p-c}}\right)}{kp} & -\frac{cq}{p} \\ \frac{2r\left[k(p-c)-\sqrt{ac(p-c)}\right]}{kq} & 0 \end{pmatrix}. \tag{5}$$

The characteristic equation of (5) is

$$\lambda^2 - \operatorname{tr}(J)\lambda + \det(J) = 0, \tag{6}$$

where the trace $\operatorname{tr}(J)$ and the determinant $\det(J)$ of J are

$$\operatorname{tr}(J) = \frac{r\left(k\left(2c-p\right)-2c\sqrt{\frac{ac}{p-c}}\right)}{kp},$$

$$\det(J) = \frac{2cr\left(k(p-c)-\sqrt{ac(p-c)}\right)}{kp} = \frac{2cr\sqrt{p-c}\left(k\sqrt{p-c}-\sqrt{ac}\right)}{kp} > 0.$$

If $a \geq k^2$ holds, it follows from $p > c\left(1+\frac{a}{k^2}\right)$ that $p > 2c$, and hence $\operatorname{tr}(J) < 0$. If (H_2) holds, then $\operatorname{tr}(J) < 0$. This completes the proof. □

Next, we consider the stability of E^* for PDE model (2). For simplicity, we only consider the special case of 2-dimensional space.

Theorem 2.2 *If the conditions* $(H1)$ *or* $(H2)$ *of Theorem* 2.1 *hold, for PDE model* (2), *the positive equilibrium* E^* *is stable.*

Proof Let $u = u^* + \tilde{u}$, $v = v^* + \tilde{v}$, where $|\tilde{u}| \ll 1$, $|\tilde{v}| \ll 1$. Thus, we add a small spatiotemporally inhomogeneous perturbation near E^* and obtain the following linear system:

$$\begin{cases} \frac{\partial \tilde{u}}{\partial t} = d_1 \Delta \tilde{u} + J_{11}\tilde{u} + J_{12}\tilde{v}, \\ \frac{\partial \tilde{v}}{\partial t} = d_2 \Delta \tilde{v} + J_{21}\tilde{u} + J_{22}\tilde{v}. \end{cases} \tag{7}$$

According to [22], any solution of system (7) can be expanded into a Fourier series as follows:

$$\begin{cases} \tilde{u}(\boldsymbol{r}, t) = \sum_{n,m=0}^{\infty} \tilde{u}_{nm}(\boldsymbol{r}, t) = \sum_{n,m=0}^{\infty} \alpha_{nm}(t) \sin(\boldsymbol{w} \cdot \boldsymbol{r}), \\ \tilde{v}(\boldsymbol{r}, t) = \sum_{n,m=0}^{\infty} \tilde{v}_{nm}(\boldsymbol{r}, t) = \sum_{n,m=0}^{\infty} \beta_{nm}(t) \sin(\boldsymbol{w} \cdot \boldsymbol{r}), \end{cases} \tag{8}$$

where $\boldsymbol{r} = (x, y)$ and $0 < x < L$, $0 < y < L$. $\boldsymbol{w} = (w_n, w_m)$ and $w_n = n\pi/L$, $w_m = m\pi/L$ are the corresponding wave-numbers. Substituting (8) into (7), we have

$$\begin{cases} \dfrac{\mathrm{d}\alpha_{nm}}{\mathrm{d}t} = (J_{11} - d_1 w^2)\alpha_{nm} + J_{12}\beta_{nm}, \\ \dfrac{\mathrm{d}\beta_{nm}}{\mathrm{d}t} = J_{21}\alpha_{nm} - d_2 w^2 \beta_{nm}, \end{cases} \tag{9}$$

where $w^2 = w_n^2 + w_m^2$.

In general, the solution of model (9) is $K_1 e^{\lambda_1 t} + K_2 e^{\lambda_2 t}$, where K_1 and K_2 are determined by the initial conditions of frPDE model (3) and λ_1 and λ_2 are the eigenvalues of the Jacobian matrix:

$$J(w) = \begin{pmatrix} J_{11} - d_1 w^2 & J_{12} \\ J_{21} & -d_2 w^2 \end{pmatrix}. \tag{10}$$

The characteristic equation of (10) is

$$\lambda^2 - \mathrm{tr}(J(w))\lambda + \det(J(w)) = 0, \tag{11}$$

where

$$\begin{aligned} \mathrm{tr}(J(w)) &= \mathrm{tr}(J) - (d_1 + d_2)w^2, \\ \det(J(w)) &= d_1 d_2 w^4 - d_2 \mathrm{tr}(J) w^2 + \det(J). \end{aligned}$$

It follows from Theorem 2.1 that $\mathrm{tr}(J(w)) < 0$ and $\det(J(w)) > 0$. Therefore, the positive equilibrium E^* of the PDE model (2) is always stable for any wave-numbers w. □

Remark 2.3 From Theorem 2.2, obviously, there is no effect of the diffusion on the stability of the positive equilibrium E^* of PDE model (2). That is to say, there is no diffusion-driven instability, i.e., Turing instability, in PDE model (2).

2.2 The case of fractional-order model

We first give the definition called fraction-diffusion-induced instability as follows.

Definition 2.4 If the positive equilibrium E^* is stable in the cases of PDE model (2) and frODE model (4), but unstable with respect to solutions of frPDE model (3), then this instability is called as fraction-diffusion-induced instability.

Now we study the stability of frODE model (4). The stability of the positive equilibrium E^* can be determined by linearizing frODE model (4) around it, which leads to the following linear system:

$$\begin{cases} \dfrac{\mathrm{d}^\eta u}{\mathrm{d}t^\eta} = J_{11}u + J_{12}v, \\ \dfrac{\mathrm{d}^\eta v}{\mathrm{d}t^\eta} = J_{21}u, \end{cases}$$

It follows from [23] that the positive equilibrium E^* is locally asymptotically stable if all the eigenvalues λ of the Jacobian matrix J evaluated at the equilibrium point satisfies

$$|\arg\lambda| > \frac{\eta\pi}{2}, \tag{12}$$

where $\lambda = \alpha \pm i\beta$ are the roots of (6) with $\beta \geq 0$. If the positive equilibrium E^* of ODE model (1) is stable, i.e., $\alpha < 0$, then $|\arg\lambda| = \arctan\frac{\beta}{\alpha} + \pi > \frac{\eta\pi}{2}$ holds. If $\alpha = 0$, $|\arg\lambda| = \frac{\pi}{2} > \frac{\eta\pi}{2}$ always holds. In this case, it follows that $\mathrm{tr}(J) = 0$. Therefore, we only need to consider the case of $\alpha > 0$, $\beta > 0$, that is $\mathrm{tr}(J) > 0$ and $4\det(J) - \mathrm{tr}^2(J) > 0$. Clearly, (12) is equivalent to

$$\tan(\arg\lambda) = \frac{\beta}{\alpha} = \frac{\sqrt{4\det(J) - \mathrm{tr}^2(J)}}{\mathrm{tr}(J)} > \tan\left(\frac{\eta\pi}{2}\right). \tag{13}$$

And hence, we can directly obtain the following results according to (13).

Theorem 2.5 *For frODE model* (4), *if*

$$\begin{aligned} &a < k^2, \quad kp + 2c\sqrt{\frac{ac}{p-c}} < 2kc \quad \textit{and} \\ &\sqrt{4ckpr\sqrt{p-c}\left(k\sqrt{p-c} - \sqrt{ac}\right) - r^2\left(k(2c-p) - 2c\sqrt{\frac{ac}{p-c}}\right)^2} \\ &\quad > r\left(k(2c-p) - 2c\sqrt{\frac{ac}{p-c}}\right)\tan\left(\frac{\eta\pi}{2}\right) \end{aligned} \tag{14}$$

hold, then the positive equilibrium E^* is stable.

Remark 2.6 Easy to prove that, if $a < k^2$, $kp + 2c\sqrt{\frac{ac}{p-c}} < 2kc$, and

$$\begin{aligned} &\sqrt{4ckpr\sqrt{p-c}\left(k\sqrt{p-c} - \sqrt{ac}\right) - r^2\left(k(2c-p) - 2c\sqrt{\frac{ac}{p-c}}\right)^2} \\ &= r\left(k(2c-p) - 2c\sqrt{\frac{ac}{p-c}}\right)\tan\left(\frac{\eta\pi}{2}\right) \end{aligned} \tag{15}$$

hold, then frODE model (4) undergoes a Hopf bifurcation around E^*.

We next consider the instability of the positive equilibrium E^* of frPDE model (3). Similar to (7), after linearized frPDE model (3), we have

$$\begin{cases} \dfrac{\partial^\eta \tilde{u}}{\partial t^\eta} = d_1\Delta\tilde{u} + J_{11}\tilde{u} + J_{12}\tilde{v}, \\ \dfrac{\partial \eta\tilde{v}}{\partial t^\eta} = d_2\Delta\tilde{v} + J_{21}\tilde{u} + J_{22}\tilde{v}. \end{cases} \tag{16}$$

According to [22, 24], any solution of system (16) can be expanded into a Fourier series (8). Substituting (8) into (16), we obtain

$$\begin{cases} \dfrac{\partial^\eta \alpha_{nm}}{\partial t^\eta} = (J_{11} - d_1 w^2)\alpha_{nm} + J_{12}\beta_{nm}, \\ \dfrac{\partial^\eta \beta_{nm}}{\partial t^\eta} = J_{21}\alpha_{nm} - d_2 w^2 \beta_{nm}. \end{cases}$$

The instability of the positive equilibrium E^* of frPDE model (3) is more complex. For convenience, we consider the case of $\det(J(w)) < 0$.

Notice that $\det(J(w))$ can achieve its minimum

$$\min_w \det(J(w)) = \frac{4d_1 d_2 \det(J) - d_2^2 \mathrm{tr}^2(J)}{4d_1 d_2}$$

at the critical value $w^{*2} = \dfrac{\mathrm{tr}(J)}{2d_1} > 0$. Consequently, for some wave numbers $w \neq 0$, if

$$4d_1 d_2 \det(J) < d_2^2 \mathrm{tr}^2(J), \tag{17}$$

we have $\det(J(w)) < 0$. (17) is equivalent to

$$\mathrm{tr}(J) > 2\sqrt{\frac{d_1}{d_2}\det(J)}.$$

Summarizing the discussions above, we have the following results.

Theorem 2.7 *Let* (14) *hold. For frPDE model* (3), *if*

$$\frac{r\left(k(2c-p) - 2c\sqrt{\frac{ac}{p-c}}\right)}{kp} > 2\sqrt{\frac{2d_1 cr\sqrt{p-c}\left(k\sqrt{p-c} - \sqrt{ac}\right)}{d_2 kp}} \tag{18}$$

holds, then the positive equilibrium E^* is unstable.

From $\det(J(w)) = 0$, we can determine w_1 and w_2 as

$$w_1^2 = \frac{d_2\mathrm{tr}(J) - \sqrt{d_2^2\mathrm{tr}^2(J) - 4d_1 d_2 \det(J)}}{2d_1 d_2}, \qquad w_2^2 = \frac{d_2\mathrm{tr}(J) + \sqrt{d_2^2\mathrm{tr}^2(J) - 4d_1 d_2 \det(J)}}{2d_1 d_2}.$$

In conclusion, if $w_1^2 < w^2 < w_2^2$, then $\det(J(w)) < 0$ and E^* of frPDE model (3) is unstable. That is to say, the fraction-diffusion-driven instability occurs, and frPDE model (3) may exhibit Turing pattern formation.

For the sake of studying the fraction-diffusion-induced instability of frPDE model (3) further, in Fig. 1, we give the bifurcation diagram in $a - p$ space with $r = 1$, $k = 1$, $c = 0.5$ and $q = 1$. Curve C_1 comes from the equation $a = \frac{k^2(p-c)(2c-p)^2}{4c^3}$, the Hopf bifurcation curve C_2 is determined by (15) for frODE model (4) with $\eta = 0.8$, and curve C_3 is obtained from the equality case of (18). In domain II, fraction-diffusion-induced instability occurs, in other words, Turing instability exists.

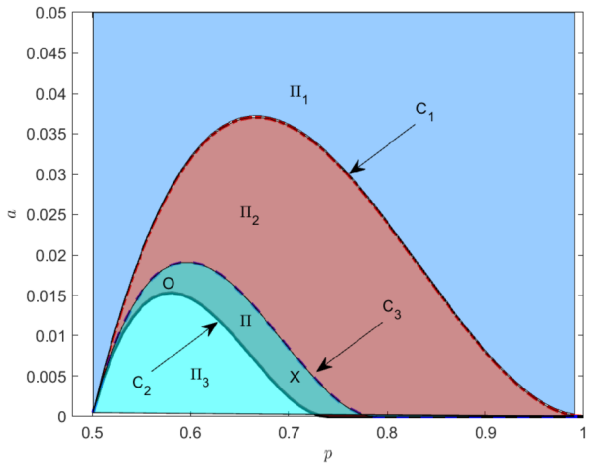

Figure 1 The bifurcation diagram of the parameters p and a for the system (4) with $r = 1$, $k = 1$, $c = 0.5$, $q = 1$, $\eta = 0.8$, the position of the mark "×" is $(p, a) = (0.701, 0.005)$, and the mark "O" is $(p, a) = (0.571, 0.0165)$

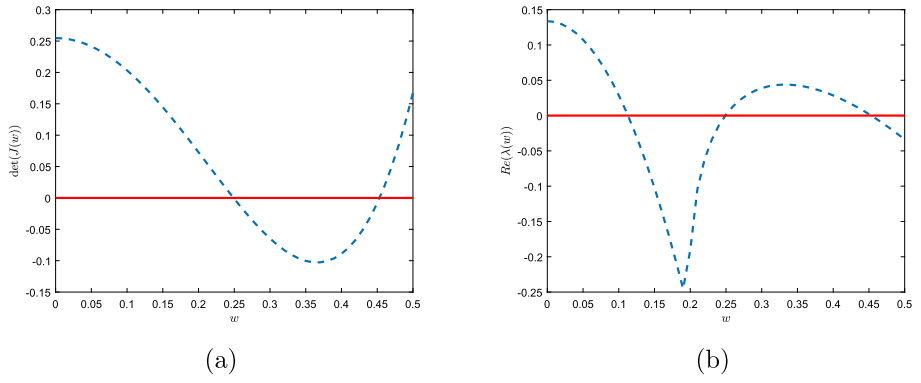

Figure 2 The dispersion coefficient and the real part of the roots in (11):(a) the suitable dispersion coefficient against the wave numbers w; (b) the real part of the characteristic roots against the wave numbers w

Furthermore, in Fig. 2, we show the existence of the wave-number w. We take the parameters as $r = 1$, $a = 0.005$, $c = 0.5$, $p = 0.701$, $k = 1$, $\eta = 0.8$ and $d_1 = 1$, $d_2 = 20$, whose position of (p, a) (marked as "×") is in the domain II of Fig. 1, and respectively plot the suitable dispersion coefficient $\det(J(w))$ of the characteristic equation (11) in Fig. 2(a) and the real part of the characteristic roots in Fig. 2(b) against the wave numbers w. We find $\det(J(w)) < 0$ and the real part $Re(\lambda(w)) > 0$ when $0.2490 < w < 0.4533$, which indicates that the Turing instability occurs.

3 Turing pattern formation

In this section, we perform extensive numerical simulations of frPDE model (3) to show the qualitative results of Turing pattern formation in two- and three-dimensional space.

3.1 Numerical method

We use the Grünwald–Letnikov method [25] to discrete the Caputo fractional-order derivative operator in system (3). The Grünwald–Letnikov fractional derivative [26] is introduced as follows.

Assume that the function $y(t)$ satisfies some smoothness conditions in every finite interval $(0,t), t \le T$. Choosing the equidistant grid

$$0 = \tau_0 < \tau_1 < \cdots < \tau_{n+1} = t,$$

and taking $h = \tau_{k+1} - \tau_k$, then the Grünwald–Letnikov fractional derivative of order η is defined by

$$ {}^{G}D_t^{\eta} y(t) = \lim_{h\to 0} \frac{1}{h^{\eta}} \Delta_h^{\eta} y(t) = \lim_{h\to 0} \frac{1}{h^{\eta}} \left(y(\tau_{n+1}) - \sum_{\nu=1}^{n+1} C_{\nu}^{\eta} y(\tau_{n+1-\nu}) \right), \tag{19}$$

where

$$C_{\nu}^{\eta} = (-1)^{\nu-1} \binom{\eta}{\nu} = \frac{-1}{\Gamma(-\eta)} \cdot \frac{\Gamma(\nu-\eta)}{\Gamma(\nu+1)},$$

and the Gamma function $\Gamma(\eta)$ is defined by the integral $\Gamma(\eta) = \int_0^{\infty} \tau^{\eta-1} e^{-\tau} \mathrm{d}\tau$.

The Grünwald–Letnikov definition based on finite differences is not equivalent to the Caputo definition. Their difference is expressed by [25]

$$ {}^{C}D_t^{\eta} y(t) = {}^{G}D_t^{\eta} y(t) - \sum_{\nu=0}^{m-1} r_{\nu}^{\eta}(t) y^{(\nu)}(0), \tag{20}$$

where $r_{\nu}^{\eta}(t) = \frac{t^{\nu-\eta}}{\Gamma(\nu+1-\eta)}$. Especially, when $0 < \eta < 1$, (20) will be simplified as

$$ {}^{C}D_t^{\eta} y(t) = {}^{G}D_t^{\eta} y(t) - r_0^{\eta}(t) y(0),$$

where $r_0^{\eta}(t) = \frac{t^{-\eta}}{\Gamma(1-\eta)}$.

From (19), when the step size $h \to 0$, the Grünwald–Letnikov approximation satisfies

$$ {}^{G}D_t^{\eta} y(t) \approx \frac{1}{h^{\eta}} \left(y(\tau_{n+1}) - \sum_{\nu=1}^{n+1} C_{\nu}^{\eta} y(\tau_{n+1-\nu}) \right).$$

Therefore, when $0 < \eta < 1$, from the following Caputo fractional-order differential equation

$$ {}^{C}D_t^{\eta} y(t) = F(y(t)), \tag{21}$$

we have

$$ \frac{1}{h^{\eta}} \left(y(\tau_{n+1}) - \sum_{\nu=1}^{n+1} C_{\nu}^{\eta} y(\tau_{n+1-\nu}) \right) - r_0^{\eta}(\tau_{n+1}) y(0) \approx F(y(\tau_n)).$$

Thus, (21) will be discretized into

$$ y(\tau_{n+1}) \approx \sum_{\nu=1}^{n+1} C_{\nu}^{\eta} y(\tau_{n+1-\nu}) + h^{\eta} r_0^{\eta}(\tau_{n+1}) y(0) + h^{\eta} F(y(\tau_n)).$$

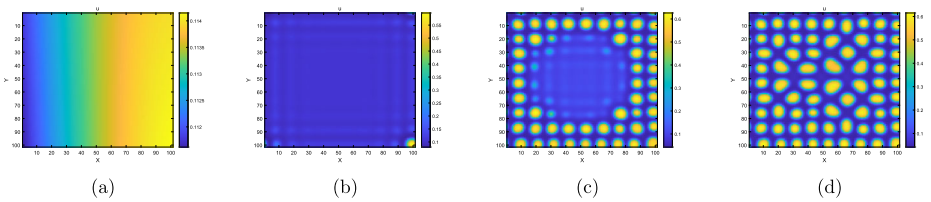

Figure 3 Turing patterns of u in 2D square domain for frPDE model (3) with initial conditions $u_0(i,j) = u^* - 2e^{-7}(x_i - 0.1y_j - L/2)(x_i - 0.1y_j - 1.5L)$, $v_0(i,j) = v^* - 3e^{-5}(x_i - L) - 1.2e^{-4}(y_j - L/3)$. Times: (a) 0; (b) 150; (c) 250; (d) 350

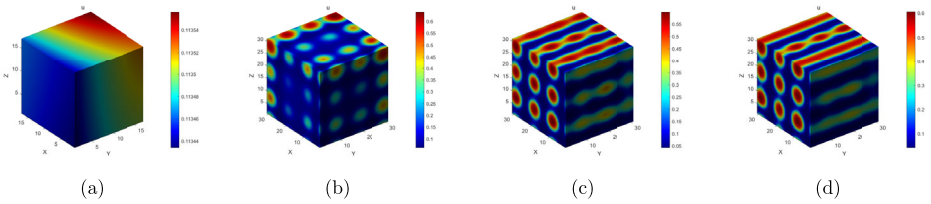

Figure 4 Turing patterns of u in 3D cube domain for frPDE model (3) with initial conditions $u_0(i,j,k) = u^* - 2e^{-7}(x_i - 0.1y_j - 0.1z_k - L/2)(x_i - 0.1y_j - 0.2z_k - 1.5L)$, $v_0(i,j,k) = v^* - 3e^{-5}(x_i - L) - 1.2e^{-4}(y_j - L/3) - 0.8e^{-4}(z_k - L/2)$. Times: (a) 0; (b) 150; (c) 250; (d) 350

3.2 Pattern formation

We take the parameters as follows:

$$r = 1, k = 1, p = 0.701, c = 0.5, a = 0.005, q = 1, d_1 = 1, d_2 = 20, \eta = 0.8.$$

For the discretization of Laplace operator, we use a 2×2 convolution matrix for 2D square domain and a $3 \times 3 \times 3$ for 3D cube domain with edge wrapping method.

In the case of two-dimensional square domain $L \times L$, we take $L = 100$, $\Delta t = 0.01$, $\Delta x = \Delta y = 1$, and the initial conditions $u_0(i,j) = u^* - 2e^{-7}(x_i - 0.1y_j - L/2)(x_i - 0.1y_j - 1.5L)$, $v_0(i,j) = v^* - 3e^{-5}(x_i - L) - 1.2e^{-4}(y_j - L/3)$. After $3.5 * 10^4$ iterations for the discrete time, the spatial two-dimensional frPDE model (3) ultimately converges to a steady state. The gradual change process of the prey's Turing patterns along time is illustrated in Fig. 3.

In the case of three-dimensional cube domain $L \times L \times L$, limited by computing power, we take $L = 30$, $\Delta x = \Delta y = \Delta z = 1$ and the other parameters as the same as the above, and the initial conditions $u_0(i,j,k) = u^* - 2e^{-7}(x_i - 0.1y_j - 0.1z_k - L/2)(x_i - 0.1y_j - 0.2z_k - 1.5L)$, $v_0(i,j,k) = v^* - 3e^{-5}(x_i - L) - 1.2e^{-4}(y_j - L/3) - 0.8e^{-4}(z_k - L/2)$. After the same iterations for the discrete time, the spatial three-dimensional frPDE model (3) ultimately converges to a steady state. The gradual change process of the prey's Turing patterns is illustrated in Fig. 4.

In addition, in order to check further Turing instability parameters, in the Turing instability region of Fig. 1, we take the parameters $p = 0.571$, $a = 0.0165$ in frPDE model (3), which is labeled in Fig. 1 with the mark "O". The other parameters are taken as the same as before. For the case of two-dimensional square domain, we take the initial conditions $u_0(i,j) = u^*$, $v_0(i,j) = v^*$ if $(x_i - L/2)^2 + (y_j - L/2)^2 < L^2/4$ and zero otherwise. For the case of three-dimensional cube domain, we take the initial conditions $u_0(i,j,k) = u^*$, $v_0(i,j,k) = v^*$

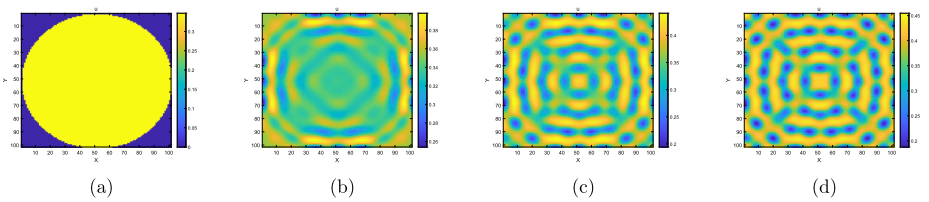

Figure 5 Turing patterns of u in 2D square domain for frPDE model (3) with initial conditions $u_0(i,j) = u^*$, $v_0(i,j) = v^*$ if $(x_i - L/2)^2 + (y_j - L/2)^2 < L^2/4$ and zero otherwise. Times: (a) 0; (b) 150; (c) 350; (d) 500

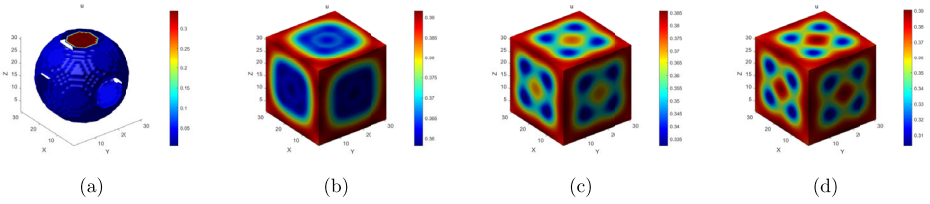

Figure 6 Turing patterns of u in 3D cube domain for frPDE model (3) with initial conditions $u_0(i,j,k) = u^*$, $v_0(i,j,k) = v^*$ if $(x_i - L/2)^2 + (y_j - L/2)^2 + (z_k - L/2)^2 < L^2/4$ and zero otherwise. Times: (a) 0; (b) 150; (c) 350; (d) 500

if $(x_i - L/2)^2 + (y_j - L/2)^2 + (z_k - L/2)^2 < L^2/4$ and zero otherwise. After a long time of calculation, the prey's Turing patterns are illustrated in Figs. 5 (2D) and 6 (3D), respectively.

4 Conclusions

In this paper, we study the spatiotemporal dynamics of a fractional-order predator-prey reaction-diffusion model with Holling-type III functional response, i.e., frPDE model (3), and obtain the conditions of fraction-diffusion-induced instability (i.e., Turing instability).

In the numerical simulation of frPDE model (3), we can easily use the Euler method to realize the iterative process. However, because of the memory and heredity of the fractional-order operator, when calculating the new iteration of fractional-order differential equations, we need to consider all the history values of the solutions. The consequence is that in the process of discretization of frPDE model (3), we have to start calculating from u_0 or v_0 for every new iteration, which leads to very large memory demand and greater computational power for the whole simulation. Meanwhile, as the spectral length L increases, the computational complexity increase also significantly. Therefore, it is necessary to use parallel computing during the simulation process.

In [18], the fractional order Laplacian operator is introduced in a three-dimensional first-order predator-prey model. The authors believe that the order of fractional diffusion affects the stability of the system pattern. This prompts us to introduce the fractional-order diffusion into our fractional-order predator-prey model in our future research.

Ruan et al [27] indicated that, the continuous random walk in the predator-prey model is a Gaussian distribution and the corresponding reaction-diffusion is the only local spatial spread of diffusion. When we deal with the cases of the long-distance geographic spread, the random Laplace diffusion certainly is not suitable to describe the spread diffusion behavior, while fractional diffusion is a more reasonable approach. That is to say, fractional diffusion has a wider range of applications than integer diffusion. In our future research, we will focus on fractional diffusion in the fractional-order population models.

Acknowledgements
This research was supported by the National Natural Science Foundation of China (Grant numbers 12071173 and 12171192) and Huaian Key Laboratory for Infectious Diseases Control and Prevention (HAP201704).

Author contributions
ZW: Modelling, mathematical analysis, numerical simulation, writing. ZWa: Modelling, numerical simulation, writing. YC: Modelling, mathematical analysis, writing. HY: Modelling, numerical simulation. WW: Modelling, mathematical analysis, writing-reviewing and editing.

Data availability
The data used to support the findings of this study are available from the corresponding author upon request.

Declarations

Competing interests
The authors declare that there are no conflicts of interest regarding the publication of this paper.

Author details
[1]School of Mathematics and Statistics, Huaiyin Normal University, Huaian, 223300, P.R. China. [2]School of Computer Science and Technology, Huaiyin Normal University, Huaian, 223300, P.R. China. [3]School of Mathematics and Statistics, Nantong University, Nantong, 226019, P.R. China. [4]School of Mathematics and Statistics, Xuzhou University of Technology, Xuzhou, 221018, P.R. China.

Received: 22 October 2024 Accepted: 10 January 2025 Published online: 04 February 2025

References

1. Turing, A.: The chemical basis of morphogenesis. Philos. Trans. R. Soc. Lond., B **237**, 37–72 (1952)
2. Medvinsky, A., Petrovskii, S., Tikhonova, I., Malchow, H., Li, B.: Spatiotemporal complexity of plankton and fish dynamics. SIAM Rev. **44**, 311–370 (2002)
3. Murray, J.D.: Mathematical Biology. Springer, New York (2003)
4. Okubo, A., Levin, S.A.: Diffusion and Ecological Problems: Modern Perspectives. Springer, New York (2001)
5. Wang, W.M., Zhu, Y., Cai, Y., Wang, W.J.: Dynamical complexity induced by Allee effect in a predator-prey model. Nonlinear Anal., Real World Appl. **16**, 103–119 (2014)
6. Chen, J., Zhang, H.: The qualitative analysis of two species predator-prey model with Holling's type III functional response. Appl. Math. Mech. **7**(1), 77–86 (1986)
7. Xie, B.F., Zhang, N.: Influence of fear effect on a Holling type III prey-predator system with the prey refuge. AIMS Math. **7**(2), 1811–1830 (2022)
8. Vishwakarma, K., Sen, M.: Influence of Allee effect in prey and hunting cooperation in predator with Holling type-III functional response. J. Appl. Math. Comput. **68**(1), 249–269 (2022)
9. Yi, F., Wei, J., Shi, J.: Bifurcation and spatiotemporal patterns in a homogeneous difusive predator–prey system. J. Differ. Equ. **246**, 1944–1977 (2009)
10. Yin, H., Wen, X.: Pattern formation through temporal fractional derivatives. Sci. Rep. **8**, 5070 (2018)
11. Angstmann, C.N., Henry, B.I., McGann, A.V.: A fractional order recovery SIR model from a stochastic process. Bull. Math. Biol. **78**, 468–499 (2016)
12. Angstmann, C.N., Erickson, A.M., Henry, B.I., et al.: Fractional order compartment models. SIAM J. Appl. Math. **77**(2), 430–446 (2017)
13. Angstmann, C.N., Erickson, A.M., Henry, B.I., Mcgann, A.V., Nichols, J.A.: A general framework for fractional order compartment models. SIAM Rev. **63**(2), 375–392 (2021)
14. Wu, Z., Cai, Y., Wang, Z., Wang, W.M.: Global stability of a fractional order SIS epidemic model. J. Differ. Equ. **352**, 221–248 (2023)
15. Owolabi, K., Agarwal, R., Pindza, E., Bernstein, S., Osman, M.: Complex Turing patterns in chaotic dynamics of autocatalytic reactions with the Caputo fractional derivative. Neural Comput. Appl. **35**, 11309–11335 (2023)
16. Carfora, M.F., Torcicollo, I.: A fractional-in-time prey-predator model with hunting cooperation: qualitative analysis, stability and numerical approximations. Axioms **10**(2), 78 (2021)
17. Zheng, Q., Shen, J., Zhao, Y., Zhou, L., Guan, L.: Turing instability in the fractional-order system with random network. Int. J. Mod. Phys. B **36**(32), 2250234 (2022)
18. Bi, Z., Liu, S., Ouyang, M.: Three-dimensional pattern dynamics of a fractional predator-prey model with cross-diffusion and herd behavior. Appl. Math. Comput. **421**, 126955 (2022)
19. Bi, Z., Liu, S., Ouyang, M., Wu, X.: Pattern dynamics analysis of spatial fractional predator-prey system with fear factor and refuge. Nonlinear Dyn. **111**, 10653–10676 (2023)
20. Owolabi, K.M., Baleanu, D.: Emergent patterns in diffusive Turing-like systems with fractional-order operator. Neural Comput. Appl. **33**, 12703–12720 (2021)
21. Yao, S., Ma, Z., Yue, J.: Bistability and Turing pattern induced by cross fraction diffusion in a predator-prey model. Phys. A **509**, 982–988 (2018)
22. Malchow, H., Petrovskii, S.V., Venturino, E.: Spatiotemporal Patterns in Ecology and Epidemiology: Theory, Models, and Simulation. Chapman and Hall/CRC, New York (2008)
23. Matignon, D.: Stability results for fractional differential equations with applications to control processing. In: Computational Engineering in Systems Applications, vol. 2, pp. 963–968. Lille (1996)
24. Lin, J., Li, J., Xu, R.: Turing instability and pattern formation of a fractional Hopfield reaction–diffusion neural network with transmission delay. Nonlinear Anal., Model. Control **27**(5), 823–840 (2022)

25. Scherer, R., Kalla, S.L., Tang, Y., Huang, J.: The Grünwald-Letnikov method for fractional differential equations. Comput. Math. Appl. **62**(3), 902–917 (2011)
26. Podlubny, I.: Fractional Differential Equations. Academic Press, New York (1999)
27. Zhao, G., Ruan, S.: Spatiotemporal dynamics in epidemic models with Lévy flights: a fractional diffusion approach. J. Math. Pures Appl. **173**, 243–277 (2023)

Publisher's Note